Acta Crystallographica Section B
Structural Science
ISSN 0108-7681

Determination of the crystal structure of the π-AlFeMgSi phase using symmetry- and site-sensitive electron microscope techniques

S. Foss,[a]* A. Olsen,[a] C. J. Simensen[b] and J. Taftø[a]

[a]Department of Physics, University of Oslo, PO Box 1048 Blindern, N-0316 Oslo, Norway, and [b]SINTEF Materials Technology, PO Box 124 Blindern, N-0314 Oslo, Norway

Correspondence e-mail: stefoss@fys.uio.no

Received 2 September 2002
Accepted 11 December 2002

The crystal structure of the complex π-AlFeMgSi phase, which was previously thought to have the composition $Al_8FeMg_3Si_6$, has been investigated. Microprobe analysis revealed that the phase has a different composition, $Al_9FeMg_3Si_5$. The space group was determined and confirmed to be $P\bar{6}2m$ with the use of parallel-beam electron diffraction (SAD) and convergent-beam electron diffraction (CBED). Owing to symmetry considerations the elements within the unit cell had to be rearranged. The rearrangement was confirmed using electron channelling. The z parameters of the elements were refined by examining the intensities from high-angle convergent-beam electron diffraction. Finally, the x parameters were adjusted slightly to arrive at acceptable interatomic distances.

1. Introduction

The crystal structure of the quarternary π-AlFeMgSi phase was originally studied by Perlitz and Westgren; its composition, space group ($P\bar{6}2m$) and atomic positions were published in 1942 (Perlitz & Westgren, 1942). According to these authors, there was a disagreement between the composition value of the π-phase as determined by weighting and by analyses. The $Al_8FeMg_3Si_6$ composition selected was a mean value. In Perlitz and Westgren's X-ray diffraction study, the space group was not determined uniquely. Of three possible space groups, one was selected because it gave the most reasonable structure. The purpose of the present study was to reinvestigate the crystal structure of π-AlFeMgSi. The π-AlFeMgSi phase is the only known quarternary phase in the Al–Fe–Mg–Si system. This phase occurs in aluminium alloys that are alloyed with a high content of silicon and magnesium, and with iron, that is present in most commercial alloys. In the absence of Mg, more than 1 wt% Si is an adequate amount to form β-AlFeSi particles. These particles have a detrimental effect on the mechanical properties of the alloy (Cáceres *et al.*, 1999). If magnesium is added to the alloy, the β-particles will not form and π-AlFeMgSi particles form instead. These particles have been reported by Cáceres *et al.* (1999) to give a lower ductility than β-AlFeSi particles.

A previous electron-microprobe investigation by Simensen & Rolfsen (1997) has indicated that the composition reported by Perlitz & Westgren (1942) may not be correct. Because of the importance of the π-phase in many aluminium alloys and the uncertainty about its composition, it was decided to carry out a new structure investigation of the π-phase. The strategy in the present work was first to determine the composition of the π-AlFeMgSi phase and then to test the original structure proposal by Perlitz & Westgren (1942) with three modern transmission electron-microscope techniques. The first of these methods, convergent-beam electron diffraction

Table 1
Structure data of the π-AlFeMgSi phase as proposed by Perlitz & Westgren (1942).

Element	Wykoff notation and number of positions	Symmetry	x	y	z
Fe	1*a*	$\bar{6}2m$	0.0	0.0	0.0
Al	1*b*	$\bar{6}m2$	0.0	0.0	0.5
Al	3*f*	*m*2*m*	0.403	0.0	0.0
Mg	3*g*	*m*2*m*	0.444	0.0	0.5
Al	4*h*	3	0.333	0.667	0.231
Si	6*i*	*m*	0.750	0.0	0.222

(CBED), was used to determine the symmetry of the crystal. Secondly we used ALCHEMI (atom location by channelling enhanced microanalysis; Taftø & Spence, 1982) to determine the location of different elements in the unit cell. ALCHEMI is a powerful technique as the X-ray and electron scattering factors for Al, Si and Mg are fairly similar. Diffraction can provide information about the position of the atoms in the unit cell but not about which atoms are located on these sites in the π-phase. The third and last method involves the use of a convergent electron beam to provide information that could enable us to determine the atom locations more exactly. The structure proposal of Perlitz & Westgren (1942) is given in Table 1. The unit cell is hexagonal with $a = 6.64$ and $c = 7.92$ Å.

2. Specimen preparation

Three ingots of different compositions, referred to as *P*1, *P*2 and *P*3, were cast (see Table 2). Samples were taken from each alloy ingot and prepared for microprobe investigation by polishing the material down to a roughness of 1 µm. Each specimen was covered with a thin layer of sputtered graphite to provide conductivity. A Cameca SX-100 electron microprobe was used.

From ingot *P*1, samples were prepared for transmission electron microscopy. The samples were thinned down to 50 µm using SiC paper and water cooling. The samples were then ion milled with a Gatan 600 ion mill using ionized argon. A Jeol 2000FX transmission electron microscope at 200 keV was used for the TEM work. Energy-dispersive X-ray spectroscopy (EDS) was carried out with a Tracor Northern detector and a ScandNordax X-ray analysis system.

3. Composition of the π-phase from electron microprobe analysis

The microprobe analysis from the three different alloys *P*1, *P*2 and *P*3 showed no large differences in composition of the π-phase. The result of the composition analysis is given in Table 3 and is in excellent agreement with the result of Simensen & Rolfsen (1997). The π-phase seems to be stoichiometric with formula $Al_9FeMg_3Si_5$, which deviates from the composition assumed by Perlitz & Westgren (1942).

Table 2
Nominal composition of alloys as determined by weighting.

Ingot	at% Al	at% Fe	at% Mg	at% Si
*P*1	72	1	9	18
*P*2	75	7.5	7.5	10
*P*3	75	7.5	2.5	15

Table 3
Microprobe analysis of π-AlFeMgSi phase crystals.

Alloy	at% Al	at% Fe	at% Mg	at% Si
*P*1	50 (1)	5.3 (0.2)	16.0 (0.3)	29 (1)
*P*2	50 (1)	5.7 (0.2)	16.6 (0.3)	28 (1)
*P*3	50 (1)	5.5 (0.2)	16.4 (0.3)	29 (1)
$Al_9FeMg_3Si_5$	50.0	5.6	16.7	27.8

4. Space group determination by convergent-beam electron diffraction (CBED)

Fig. 1 shows selected area and convergent-beam electron diffraction patterns.

The selected area diffraction patterns are consistent with a hexagonal Bravais lattice with unit-cell parameters $a = 6.6$ and $c = 7.9$ Å. Owing to the low precision in the determination of cell dimensions with electron diffraction, the experimental SAD patterns may also be consistent with triclinic, monoclinic and orthorhombic Bravais lattices. In order to distinguish these possibilities and determine possible point groups and/or space groups, convergent-beam electron diffraction (CBED) was used (Buxton *et al.*, 1976). The CBED patterns with the incident electron beam along the [001] direction show 3*m* whole-pattern (WP) symmetry (Fig. 1*d*). The [010] CBED patterns exhibit 2*mm* whole-pattern symmetry (Fig. 1*e*). From these CBED patterns, the space group $P\bar{6}2m$ (No. 189) could be uniquely determined as shown in Fig. 2. According to the figure, the only common point groups that are consistent with both [001] and [010] projections are $\bar{6}m2$, *m*3*m* and $\bar{4}3m$. Because a cubic Bravais lattice is not consistent with the SAD patterns, we are left with the point group $\bar{6}m2$. A comparison of the [001] SAD and CBED patterns shows that the mirror lines in Fig. 1(*d*) are normal to the $\langle 100\rangle^*$ directions. Thus the only possible space group is $P\bar{6}2m$ (No. 189).

5. Electron channelling, ALCHEMI

Our electron diffraction study has confirmed the Bravais lattice and cell dimensions reported by Perlitz & Westgren (1942), and we have unambiguously determined that the space group proposed by these investigators is the correct one. However, a previous (Simensen & Rolfsen, 1997) and the present electron microprobe analysis suggest the composition $Al_9FeMg_3Si_5$ rather than the composition $Al_8FeMg_3Si_6$, on which Perlitz and Westgren based their structure determination. The revised composition is incompatible with an ordered alloy with the site assignment reported by Perlitz & Westgren (1942). This discrepancy can be reconciled by the following changes: Al is replaced by Si in the positions 1*b* and 4*h* and Si

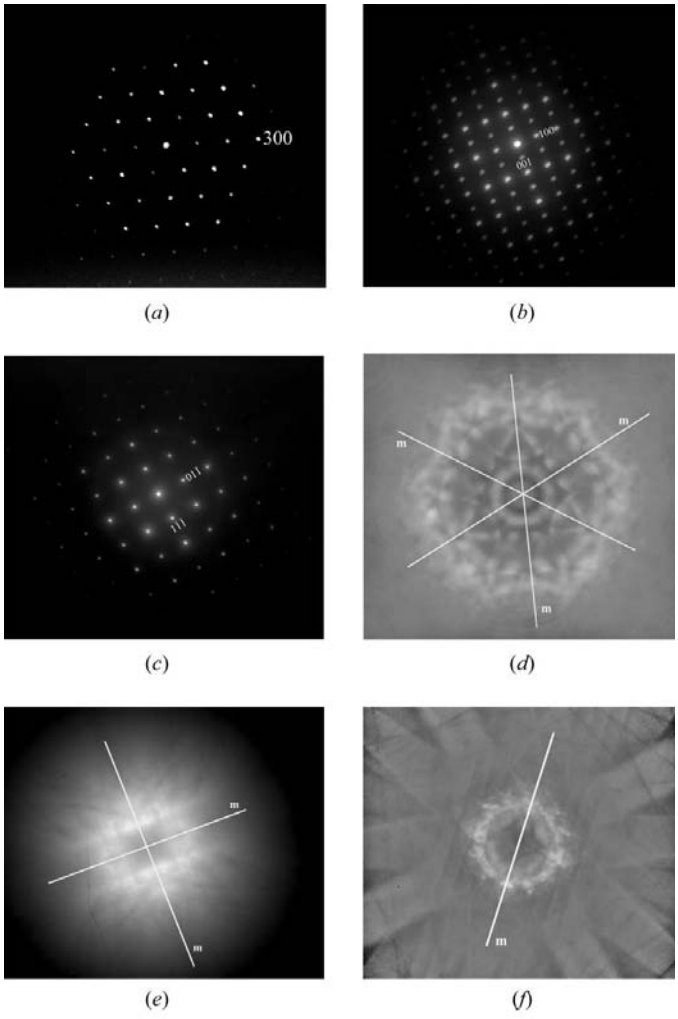

Figure 1
Parallel-beam diffraction (or SAD) of a π-phase crystal, with the incident electron beam parallel to (*a*) the [001] direction, (*b*) the [010] direction and (*c*) the [211] direction, and the corresponding convergent-beam electron diffraction patterns (*d*, *e* and *f*).

by Al in 6*i* (see Fig. 3). The task in the following is to experimentally test the new model against the original one.

The X-ray and electron scattering amplitudes of Mg, Al and Si, which are neighbours in the periodic system, have similar values. Thus it is difficult to distinguish between these atoms with X-ray and electron-diffraction intensity data. One technique that is capable of distinguishing neighbours in the periodic table is ALCHEMI, a technique based on electron channelling (Taftø & Spence, 1982). The electron-induced X-ray emission is detected using EDS when the electrons channel through the thin specimen. Electron channelling takes place when the incident plane wave of electrons enters the crystal nearly parallel to crystal planes or axes, giving rise to planar or axial electron channelling. A modulation of the wavefield builds up as the electrons propagate through the thin crystal. A brief preliminary report of the application of the ALCHEMI technique on this particular system is given elsewhere (Foss *et al.*, 2003).

We performed planar channelling experiments with the incident electron beam parallel to the (001), (100) and (110) planes. The sequence of atomic planes, based on the original and proposed new model, under these three experimental conditions is shown in Figs. 4(*a*)–4(*c*). The calculated wavefield modulation when the incident electron beam is parallel to the atomic planes is also shown. The method of calculating the wavefield modulation was based on Bloch waves (Howie, 1970) and the scattering factors of Doyle & Turner (1968).

The X-ray emission increases with increasing thickness-averaged electron current density at an atom. Thus, irrespective of model, we expect from Figs. 4(*a*)–4(*c*) an enhancement in X-ray emission from Fe for all these planar channelling conditions where the electrons enter parallel to the atomic planes. We compared the channelling spectra with spectra taken without channelling, *i.e.* a uniform wavefield over the repeat unit of the projected structure. These spectra were obtained by tilting the incident beam a few degrees so that

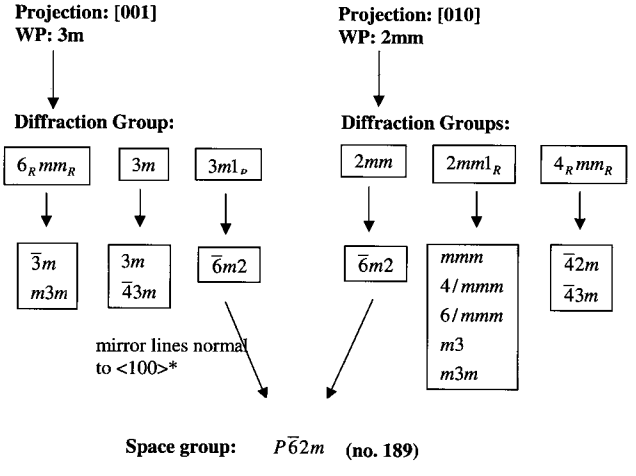

Figure 2
The determination of the space group of the π-phase.

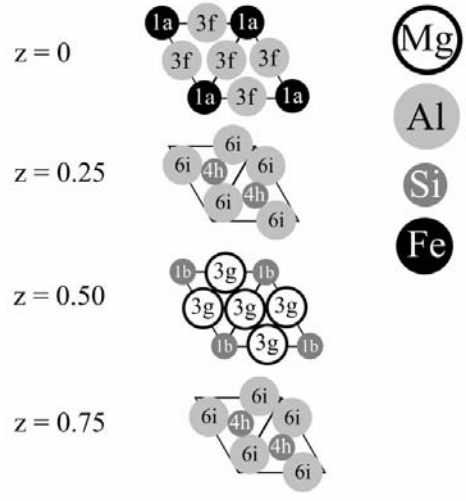

Figure 3
Atomic configuration within the π-AlFeMgSi unit cell.

strong Kikuchi bands appeared in the diffraction pattern. X-ray spectra for the planar channelling are shown in Figs. 5(*a*)–5(*c*). An X-ray spectrum obtained without channelling is shown in Fig. 5(*d*). These spectra confirm the enhancement of X-ray emission from Fe with the incident beam parallel to the atomic planes.

It is difficult to normalize two spectra so that they can be easily compared. The ratios between the X-ray yields for the different elements for a channelling and a non-channelling condition were compared to circumvent this problem. These ratios are shown for three sets of measurements, using a parameter R_x:

$$R_x = \left(N_{x,\mathrm{ch}}/N_{x,\mathrm{non}}\right)/\left(N_{\mathrm{Fe,ch}}/N_{\mathrm{Fe,non}}\right), \qquad (1)$$

where x denotes the element, $N_{x,\mathrm{ch}}$ is the number of X-ray counts from element x when channelling occurs, and $N_{x,\mathrm{non}}$ is the number of X-ray counts when the beam is tilted away from the channelling condition.

In Table 4 we present R_x for several measurements for the three sets of planes. Here R_{Fe} is unity by definition, while R_{Mg}, R_{Al} and R_{Si} are less than 1. The exception is R_{Si} for channelling from (110), which is also 1 within the experimental error. Considering the sequences of atomic planes for the two models, only in one case are all the atoms of one of the light elements on the same plane as the Fe atoms; this result is obtained for channelling from the (110) planes where the Si and Fe atoms are located in the same plane in the new proposed model. Thus, under these experimental conditions, the Si atoms are exposed to the same wavefield as the Fe

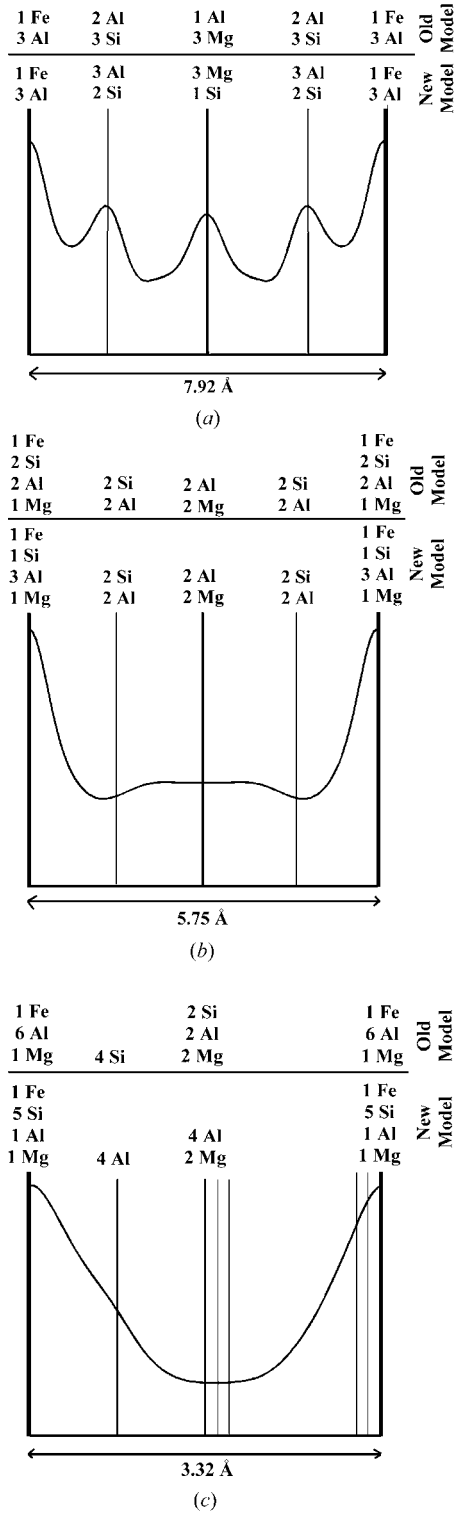

Figure 4
Wavefield of the electron beam calculated when the incident electron beam is parallel to (*a*) the (001) plane, (*b*) the (100) plane and (*c*) the (110) plane. Note that in the new model the Fe and Si atoms lie in the same plane in (*c*) (the plane represented by the thick line).

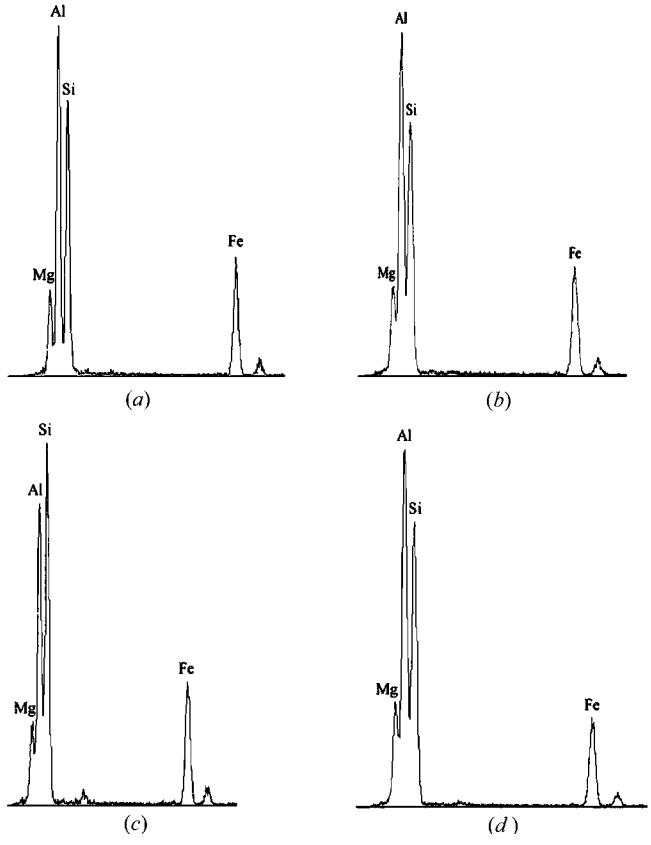

Figure 5
X-ray spectra with the incident electron beam parallel to (*a*) the (001) planes, (*b*) the (100) planes and (*c*) the (110) planes and (*d*) when strong Bragg reflections are avoided.

Table 4
R values obtained from channelling experiment using an electron beam parallel to the (001), (001) and (110) planes.

For each of the planes we present two sets of measurements. Accuracy is 10%.

	001		100		110	
Element	*R*	*R*	*R*	*R*	*R*	*R*
Al	0.57	0.57	0.59	0.68	0.61	0.77
Fe	1	1	1	1	1	1
Mg	0.53	0.59	0.52	0.72	0.59	0.73
Si	0.62	0.68	0.67	0.73	0.96	1.00

atoms, and we expect $R_{Si} = 1$ in agreement with observations in Table 4. Therefore the old model of the structure can be ruled out, while the channelling observations are consistent with the new model.

6. High-angle convergent-beam electron diffraction

The interatomic distances that Perlitz & Westgren (1942) reported, based on their semiquantitative experimental data for the determination of the coordinates of atoms at general positions, were reasonable. However, now there is strong evidence from ALCHEMI that Si and Al atoms have to interchange positions. The larger Al atoms are too close to their neighbouring atoms unless we adjust the coordinates of atoms in general positions.

The components of the position parameters parallel to a dense reciprocal lattice row can be conveniently tested by convergent electron diffraction by orienting the crystal so that many reflections along the dense row are at the Bragg position simultaneously (Taftø & Metzger, 1985) (see Fig. 6). The diffraction intensities in this case are not formed as spots but as lines, similar to Kikuchi lines. The intensities of these lines are based on two-beam coupling, because the Ewald sphere is steep for large *g*–vectors. Thus, coupling to other reflections along this reciprocal row is weak. For thin crystals, the diffraction intensities scale as $|F_g|^2$. The structure factors F_g are sensitive to small changes of the atomic-position parameters for high scattering angles. We used this technique to obtain information about the *z* parameter of the atoms located at sites 6*i* and 4*h*. All measured 00*l* intensities have to be far out into reciprocal space. In such a case, diffraction occurs only over a narrow angular range around the exact Bragg position.

Fig. 7 shows the CBED pattern acquired for a setup like that in Fig. 6. The lines represent intensities. Fig. 8 shows the corresponding measured intensities for reflections along the [001]* direction. For $l = 12$, the intensity is quite high. The intensities are generally high for $l = 4n$ because of the four-

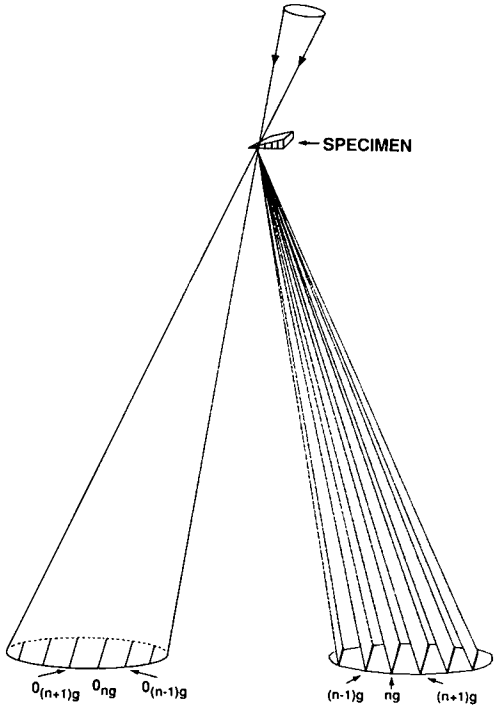

Figure 6
High-angle convergent-beam diffraction. Allows for many reflections at the Bragg angle within one disc (Taftø & Metzger, 1985) for large scattering angles.

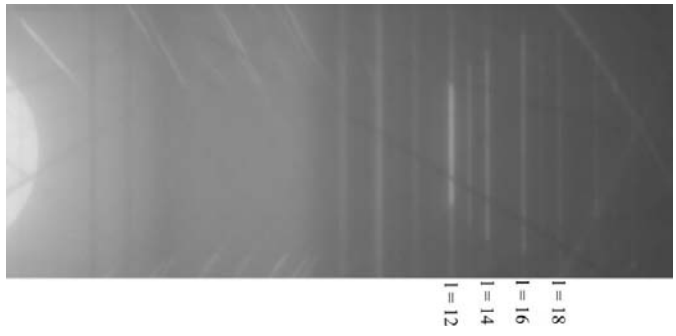

Figure 7
High-angle convergent-beam electron diffraction, where the beam is tilted from a position parallel to the (001) planes.

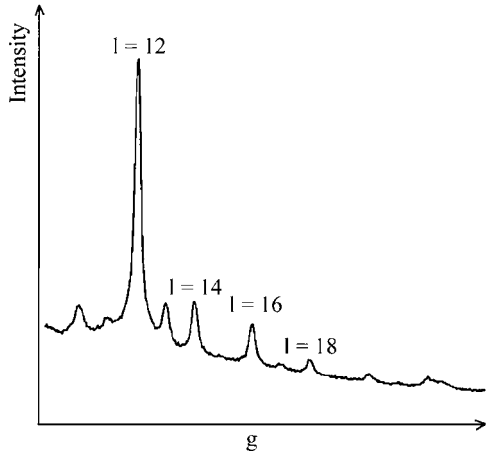

Figure 8
Measured intensities during high-angle convergent-beam electron diffraction. Reflections are in the [001]* direction. The intensity scale is arbitrary.

layer structure in the [001] direction. The corresponding calculations for different arrangements of the atoms in the unit cell are shown in Figs. 9(*a*)–9(*d*). We demonstrate in Figs. 9(*a*) and 9(*b*) the sensitivity to small changes in the *z* parameters of the atoms in the 4*h* and 6*i* positions. The proposal of Perlitz & Westgren (1942), which is shown in Table 1, does not fit that far out in reciprocal space (Fig. 9*c*). A good fit was obtained for $z = 0.266$ for Si atoms in position 4*h* and $z = 0.236$ for Al atoms in position 6*i* (Fig. 9*d*).

7. Discussion

The structure of the π-phase must also agree with other chemical observations, and the distance between the atoms must be larger than certain minimum values. Investigations (Massalski, 1990) of Mg–Fe alloys have shown that the solubilities of Fe in Mg and of Mg in Fe are both extremely low. No intermetallic Mg–Fe phase has been detected. Thus it is expected that there will be no Fe atoms close to Mg atoms in the π-phase. Secondly, binary phases show that the distance between several of the mentioned elements is smaller than the distance estimated on a 'hard' sphere model of atoms. The distance between Al and Fe is only 0.251 nm in $AlFe_3$ (Villars & Galvert, 1967; Mondolfo, 1976). The corresponding value for (*a*) Al—Mg is 0.297 nm ($Mg_{17}Al_{12}$), (*b*) Mg—Si is 0.274 nm (Mg_2Si) and (*c*) Si—Fe is 0.234–0.235 nm (SiFe and $SiFe_3$).

The microprobe analysis and the SAD and CBED diffraction data showed that the π-phase has space-group symmetry No. 189 (*International Tables for Crystallography*, 1992) and a unit cell with 18 atoms and composition Al_9FeMg_3Si. Measurements using ALCHEMI revealed that atoms must be in the following positions: Fe in the 1*a* site, Si in the 1*b* site, Al in the 3*f* sites, Mg in the 3*g* sites, Si in the 4*h* sites and Al in the 6*i* sites. CBED analysis showed that a good fit to the observed diffraction intensities at a high *g* value was obtained for $z = 0.266$ for Si atoms in position 4*h* and $z = 0.236$ for Al atoms in position 6*i*. Because we used only a row of reflections along the *z* axis, only the *z* parameters could be determined by this CBED technique. When the interatomic distances were calculated, it was found that some distances were too short. Therefore, the *x* components of some atom positions were adjusted slightly. Since Al—Fe and Mg—Si make close bonds in binary phases, these atoms were displaced, which resulted in the unit cell described in Table 5. This crystal structure obeys reasonably well the rule of a minimum distance between atoms according to empirical data from binary crystals and crystals of pure elements.

This study was motivated by a new determination of the composition of the π-AlFeMgSi phase, which was found to be $Al_9FeMg_3Si_5$ from accurate electron-microprobe analysis. From this new knowledge, we were able to determine the

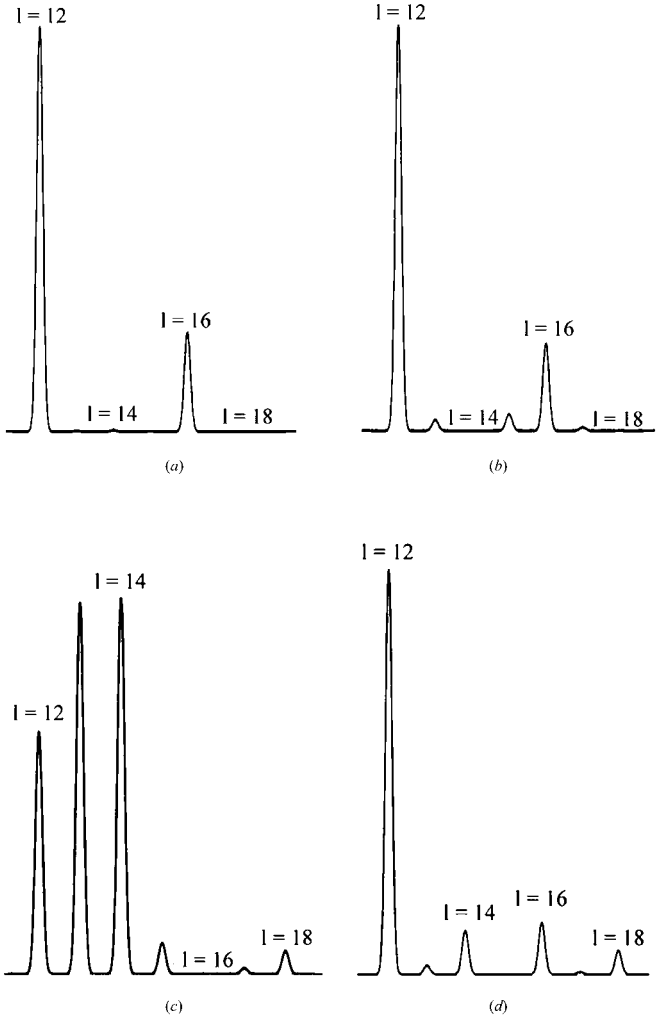

Figure 9
Calculated 001 structure factors for the π-AlFeMgSi phase assuming (*a*) $z = 0.250$ at 6*i* and $z = 0.250$ at 4*h*, (*b*) $z = 0.250$ at 6*i* and $z = 0.260$ at 4*h*, (*c*) $z = 0.222$ at 6*i* and $z = 0.231$ at 4*h* [Perlitz & Westgren's (1942) suggestion], and (*d*) $z = 0.236$ at 6*i* and $z = 0.266$ at 4*h* (suggested for the present model).

Table 5
Structure parameters and interatomic distances of the π-phase.

Atom	Number/ Position	Coordinates *x*	*y*	*z*	Surrounding atoms	Distance (nm)
Fe	1*a*	0	0	0	3 Al in *f*	0.251
					6 Al in *i*	0.248
Si	1*b*	0	0	0.5	3 Mg in *g*	0.285
					6 Al in *i*	0.267
Al	3*f*	0.378	0	0	1 Fe in *a*	0.251
					4 Si in *h*	0.296
					2 Al in *i*	0.302
Mg	3*g*	0.43	0	0.5	3 Si in *b*	0.285
					3 Mg in *g*	0.341
					4 Si in *h*	0.271
					2 Al in *i*	0.298
Si	4*h*	1/3	2/3	0.266 (5)	3 Al in *f*	0.296
					3 Mg in *g*	0.271
					3 Al in *i*	0.258
Al	6*i*	0.755	0	0.236 (5)	1 Fe in *a*	0.248
					1 Si in *b*	0.267
					1 Al in *f*	0.302
					1 Mg in *g*	0.341
					2 Si in *h*	0.258
					2 Al in *i*	0.282

crystal structure using advanced transmission electron microscopy techniques including SAD, CBED, ALCHEMI and high-angle convergent-beam electron diffraction.

This project was in part financed by the Norwegian Research Council through the FIN (Films, Interfaces and Nanomaterials) project.

References

Buxton, B. F., Eades, J. A., Steeds, J. W. & Rackham, G. M. (1976). *Philos. Trans. R. Soc. London Ser A*, **281**, 171–194.
Cáceres, C. H., Davidson, C. J., Griffiths, J. R. & Wand, Q. G. (1999). *Metall. Mater. Trans.* **30**A, 2611–2617.
Doyle, P. A. & Turner, P. S. (1968). *Acta Cryst.* A**24**, 390–397.
Foss, S., Simensen, C. J., Olsen, A. & Tafto, J. (2002). *Philos. Mag. Lett.* **82**, 681–686.
Howie, A. (1970). *Modern Diffraction and Imaging Techniques in Material Science*, edited by S. Amelinckx, R. Gevers, G. Remaut & J. V. Landuyt, pp. 295–306. Amsterdam: North-Holland.
Massalski, T. B. (1990). *Binary Alloy Phase Diagrams.* Ohio: ASM International.
Mondolfo, L. F. (1976). *Aluminium Alloys: Structure and Properties.* London: Butterworths.
Perlitz, H. & Westgren, A. (1942). *Ark. Kemi Mineral. Geol.* **15**B, 1–8.
Simensen, C. J. & Rolfsen, T. L. (1997). *Z. Metallkdd.* **88**, 142–146.
Taftø, J. & Metzger, T. H. (1985). *J. Appl. Cryst.* **18**, 110–113.
Taftø, J. & Spence, J. C. H. (1982). *Science*, **218**, 49–51.
Villars, P. V. & Galvert, L. D. (1967). *Pearson's Handbook of Crystallographic Data for Intermetallic Phases*, Vol. 1–3. Ohio: ASM International.